Novel network morphologies and compositionally robust 3-colored perforated lamellar phase in $A(BC)_2$ mikto-arm star copolymer melts†

Jacob Judas Kain Kirkensgaard*

Received 11th May 2010, Accepted 16th September 2010
DOI: 10.1039/c0sm00358a

Dissipative particle dynamics simulations are used to investigate the self-assembly of $A(BC)_2$ 3-mikto-arm star copolymers. The simulations predict a range of structures obtained by varying the volume fractions of the 3 components. Most notably the simulations show that a 3-colored perforated lamellar phase recently identified experimentally where the C and B components perforate lamellae of A is stable over a wide range of compositions. Further, the possibility of forming two other completely novel morphologies in this system is highlighted, one consisting of spheres of the A component and a 3-connected gyroid-like network of the C component embedded in a matrix of B and the other consisting of a single core-shell 3-connected gyroid-like network of A wrapped with B and embedded in a matrix of C. If realized experimentally, these networks potentially represent chiral structures built from achiral molecules as well as a single network analogue of an ordinary bicontinuous structure.

1 Introduction

The study of block copolymer self-assembly and micro-phase separation has been an active field of research for many years now with significant progress in the understanding of particularly its simplest representatives, the linear di- and tri-block copolymers.[1–3] Even though going from an AB diblock to a linear ABC triblock copolymer is conceptually simple, the complexity of the resulting phase diagram is dramatically increased.[4–6] The complexity increases even further when the molecular composition goes beyond linear designs and introduces branching in the copolymers as for example in mikto-arm star copolymers (see Fig. 1). In this paper we will focus on a newly designed molecule synthesized in the group of Hadjichristidis and illustrated schematically in Fig. 1(e), the $A(BC)_2$ mikto-arm star copolymer. This is a three-armed star copolymer with 2 arms being equivalent diblocks and one arm a single polymer species. This block copolymer has so far only been examined with one set of molecular weights. The experimental determination of the morphology of this sample has been done by combining simultaneous in situ shear and small-angle neutron scattering with dissipative particle dynamics (DPD) simulations, where the DPD approach was very well validated as it proved to match the experiments excellently.[7] The structure identified by both experiments and simulations is a perforated lamellar (PL) morphology described in detail below. Due to its topology, PL structures have interesting perspectives as functional soft materials since one might selectively remove one component and thus for example generate continuous structures with well-defined nanopores.[8] PL phases have received considerable interest in diblock copolymer systems, particularly the question of whether it is a thermodynamically stable phase.[9–25] Here we present DPD simulations indicating that by increasing the molecular complexity one can increase the stability of such otherwise transient and difficultly obtainable structures. Specifically, we significantly expand the above mentioned simulations[7] and investigate the role of molecular architecture by tuning the relative volume fractions in the system in order to clarify the compositional stability of the PL phase as well as look for potential new mesoscopic patterns in this novel polymer system and thus guide future efforts in design and synthesis.

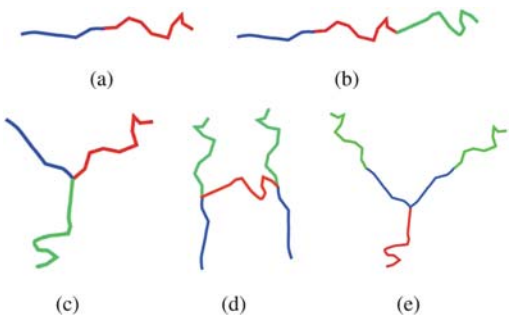

Fig. 1 Examples of block copolymer molecular designs with varying structural complexity. (a) AB diblock (b) Linear ABC triblock (c) Star-shaped ABC mikto-arm (d) H-shaped (AC)B(CA) mikto-arm (e) Star-shaped $A(BC)_2$ mikto-arm.

2 Simulation details

We briefly summarize the details of the DPD implementation employed here and refer to previous work for further discussion of the algorithm.[26–29] The time evolution of an ensemble of DPD particles is found by solving Newton's equations of motion. The i'th particle experiences a pairwise additive force $\mathbf{F}_{ij} \equiv \mathbf{F}(r_{ij})$ with a conservative, a dissipative and a random component

$$\mathbf{F}_{ij} = \sum_{i \neq j} \mathbf{F}_{ij}^{C} + \mathbf{F}_{ij}^{D} + \mathbf{F}_{ij}^{R} \quad (1)$$

with the sum running over all j particles within a cut-off radius r_c which is also considered the unit of length and set to unity. The typical DPD conservative force comes from a soft potential like

Dept. of Basic Sciences and Environment, Faculty of Life Sciences, University of Copenhagen, Denmark. E-mail: kirkensgaard@life.ku.dk
† Electronic Supplementary Information (ESI) available: Movie of perforated lamellar phase from Fig. 3. See DOI: 10.1039/c0sm00358a/

$$V^{C}(r_{ij}) = \begin{cases} \frac{a_{ij}}{2}\left(1-\frac{r_{ij}}{r_c}\right)^2 & \text{for } r_{ij} \le r_c \\ 0 & \text{for } r_{ij} > r_c \end{cases} \quad (2)$$

where a_{ij} and r_{ij} are the interaction parameter and distance between particles i and j respectively. This potential leads to a conservative force

$$\mathbf{F}_{ij}^{C} = a_{ij}\sum_{j} f_c(r_{ij})\hat{\mathbf{r}}_{ij} \quad (3)$$

with

$$f_c(r_{ij}) = \begin{cases} 1-\frac{r_{ij}}{r_c} & \text{for } r_{ij} \le r_c \\ 0 & \text{for } r_{ij} > r_c \end{cases} \quad (4)$$

and $\hat{\mathbf{r}}_{ij}$ denoting a unit vector between the two particles. The dissipative force is a hydrodynamic drag (or friction) force depending on the velocity $\mathbf{v}_{ij}$ between particles i and j and given by

$$\mathbf{F}_{ij}^{D} = \begin{cases} -\gamma\omega^{D}(r_{ij})(\hat{\mathbf{r}}_{ij}\cdot\mathbf{v}_{ij})\hat{\mathbf{r}}_{ij} & \text{for } r_{ij} \le r_c \\ 0 & \text{for } r_{ij} > r_c \end{cases} \quad (5)$$

Here γ is the friction coefficient setting the strength of the dissipative force and ω^{D} is a weight function defined below. The random force is

$$\mathbf{F}_{ij}^{R} = \sigma\omega^{R}(r_{ij})\frac{\theta_{ij}}{\sqrt{\Delta t}}\hat{\mathbf{r}}_{ij} \quad (6)$$

Again ω^{R} is a weight function, σ is the strength of the random force, Δt a time-step in the integration algorithm and θ_{ij} a Gaussianly distributed random variable different for each particle pair and without memory (*i.e.* it changes after each time step). The random force mimics a thermal noise and together with the friction force acts as a thermostat (as a heat source and sink respectively). The weight functions and constants from the dissipative and random forces are related by

$$\sigma^2 = 2\gamma k_B T \quad (7)$$

and

$$\omega^{D} = [\omega^{R}]^2 \quad (8)$$

ensuring that the fluctuation-dissipation theorem is satisfied[27] and with the weight function usually taken as

$$\omega^{D} = \begin{cases} (r_c - r_{ij})^2 & \text{for } r_{ij} \le r_c \\ 0 & \text{for } r_{ij} > r_c \end{cases} \quad (9)$$

Finally, connected beads in each molecule are held together by harmonic bonds

$$V^{S} = \frac{C}{2}(r_{ij} - r_0)^2 \quad (10)$$

with $r_0 = 1$ and $C = 4$. The integration of the equations of motion is done using a standard velocity-Verlet algorithm with time step $\Delta t = 0.01$, $k_B T = 1$, $\gamma = 4.5$ and thus $\sigma = 3$. All simulations are performed in a cubic box of volume L^3 and with particle density $\rho = 3$. Thus the number of particles in each simulation is $3L^3$. It is well known that the simulation box can induce undesirable artifacts. This can happen as a result of a too small box or if the box dimensions happen to stabilize an otherwise metastable or unstable phase. The rule of thumb in this respect is to use box sizes of at least 8–10 times the radius of gyration and to check all results in different box sizes to ensure the obtained morphology is not a box effect.[29,30] All presented results have been checked for finite size effects from the simulation box based on these criteria (details given in Table 1) with the radius of gyration R_g calculated from

$$R_g = \langle R_g^2\rangle^{\frac{1}{2}} = \left\langle \frac{1}{N}\sum_{i=1}^{N}\left|\mathbf{r}_i - \mathbf{r}_{cm}\right|^2 \right\rangle^{\frac{1}{2}} \quad (11)$$

where $\mathbf{r}_i$ and $\mathbf{r}_{cm}$ are the position vectors of the i'th bead in the molecule and the center of mass of the molecule respectively and the averaging is done over all molecules in a series of representative trajectory snapshots. Simulations were run using the

Table 1 Simulation details for CG1 results summarized in Fig. 4(a). The columns contain the number of beads in each arm (A,B,C), the box side lengths where the phase was obtained, the minimum ratio between box size and radius of gyration and the morphology found for each molecule

A	B	C	Box	Box/R_g	Morphology
0	6	5	20,24	11.1	[LAM]
1	6	5	19,21	10.6	[LAM]
1	6	5	20,24,25,26	10.9	[GL_{AB}]
2	6	5	22,23,24	12.2	[PL_A]
3	6	5	24, 28	13.2	[PL_A]
4	6	5	23,25	12.8	[PL_A]
5	6	5	25,26	13.6	[PL_A]
6	6	5	25,26,28	13.6	[PL_A]
7	6	5	25,26,27	13.5	[PL_A]
8	6	5	26,27,29	13.4	[PL_A]
9	6	5	28,30	14.7	[PL_A]
9	6	5	27	13.9	[DIA]
10	6	5	30	15.4	[PL_A]
10	6	5	27,28	13.8	[DIA]
11	6	5	26	13.2	[PL_A]
11	6	5	27,28	13.7	[DIA]
11	6	5	29	15.0	[LAM_2]
12	6	5	29,30	14.9	[LAM_2]
14	6	5	27,32	13.5	[LAM_2]
7	0	5	21	12.8	[CYL_A]
7	1	5	23,24	13.6	[CYL_A]
7	2	5	19,26	10.9	[CYL_A]
7	3	5	24,27	13.0	[CYL_A]
7	4	5	23,24	12.5	[CYL_A]
7	4	5	25,26	13.9	[PL_A]
7	5	5	26,28	14.2	[PL_A]
7	6	5	25,26,27	13.5	[PL_A]
7	7	5	27,29	14.2	[PL_A]
7	8	5	28,29	14.5	[PL_A]
7	9	5	29,30	14.7	[PL_A]
7	10	5	25,30	12.5	[PL_A]
7	11	5	26,28	12.9	[S_A + GL_C]
7	12	5	27,28,31	13.3	[S_A + GL_C]
7	6	0	20,21	12.1	[CYL_A]
7	6	1	20,21	11.9	[CYL_A]
7	6	2	23,24	13.2	[PL_A]
7	6	3	25,26	13.9	[PL_A]
7	6	4	26,27	13.6	[PL_A]
7	6	5	25,26,27	13.5	[PL_A]
7	6	6	26,27	13.2	[CYL_A]
7	6	7	26,30	13.1	[CYL_A]
7	6	8	27,30	13.5	[CYL_A]
7	6	9	29,30	14.6	[CYL_A]
7	6	10	28,32	13.5	[CYL_A]

ESPResSo package[31] within the framework developed earlier to simulate branched molecules in general.[32] Simulation snapshots and the movie (available as ESI†) were all made with the VMD package.[33]

As already mentioned this investigation took its starting point with an actual molecule and we will adopt the molecular composition of this as our reference point as shown in Fig. 2. In the real copolymer the A chain is poly(2-vinylpyridine) (P2VP), the B chain is polystyrene (PS) and the C chain polyisoprene (PI). The junction region is a small chain of polydimethylsiloxane (PDMS) which we map onto a single DPD bead. The remaining arm lengths are then determined based on the volume fractions of the experimental system as described elsewhere.[7] We present results from two different levels of coarse graining: First, relative to the reference composition we will vary all arms lengths between 0 and 2 times the reference length one by one while keeping the other arms at their reference length. The detailed results of these simulations are summarized in Fig. 4(a) and Table 1. Second, we crudely remap the reference structure to fewer beads, specifically to A_4-(B_3-C_3)$_2$, thus sacrificing compositional resolution in order to investigate longer relative lengths of each arms, again keeping the other arm lengths fixed. The detailed results from these simulations are summarized in Fig. 4(b) and Table 2. We will refer to these two levels of coarse graining as 'CG1' and 'CG2' respectively. The careful and systematic checking of box effects apply particularly to the CG1 scheme, whereas the CG2 simulations has been checked only when deemed necessary to establish certainty of the resulting equilibrium morphology. In the CG2 simulations we also increase the time step to $\Delta t = 0.02$.

At a density of $\rho = 3$ the interaction parameter between unlike particles can be related to the Flory–Huggins interaction parameter χ_{ij}[28] so that

$$a_{ij} = a_{ii} + 3.497\chi_{ij} \quad (12)$$

with the like-like interaction parameter usually determined from the compressibility of water to be $a_{ii} = 25$.[28] Here we assume symmetric interaction parameters between the different polymer species and employ $a_{ij} = 36$ which corresponds roughly to the interaction between PS and PI in a diblock copolymer of comparable size to the one building up the two BC arms of the molecule in Fig. 2.[34] However, as discussed by others,[35] the translation of the DPD interaction parameter to χ values

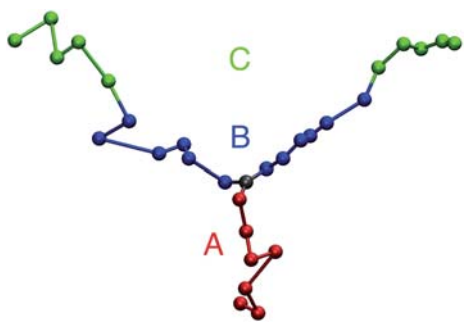

Fig. 2 Rendering of the reference model A_7-(B_6-C_5)$_2$ mikto-arm star molecule corresponding to the volume fractions of the P2VP(PDMS-*b*-PI-*b*-PS)$_2$ polymer investigated elsewhere.[7]

Table 2 Simulation details for CG2 results summarized in Fig. 4(b). The columns contain the number of beads in each arm (A,B,C), the box side lengths where the phase was obtained, the minimum ratio between box size and radius of gyration and the morphology found for each molecule

A	B	C	Box	Box/R_g	Morphology
0	3	3	20	13.4	[LAM]
1	3	3	19,20,22	12.2	[GL_{AB}]
2	3	3	20	12.9	[CYL_A]
3	3	3	20	12.5	[CYL_A]
4	3	3	21	12.8	[PL_A]
5	3	3	21	12.8	[PL_A]
6	3	3	22	13.1	[PL_A]
6	3	3	20	11.8	[DIA]
7	3	3	22	13.0	[LAM_2]
8	3	3	22	12.9	[LAM_2]
10	3	3	25	14.0	[LAM_2]
12	3	3	25	13.2	[LAM_2]
14	3	3	25	13.6	[LAM_2]
16	3	3	26	13.4	[LAM_2]
4	0	3	19	13.1	[CYL_A]
4	1	3	19	12.4	[CYL_A]
4	2	3	19,21	12.1	[CYL_A]
4	3	3	21	12.8	[PL_A]
4	4	3	22	13.1	[PL_A]
4	5	3	22	12.9	[PL_A]
4	6	3	23	13.2	[PL_A]
4	7	3	24	13.4	[PL_A]
4	8	3	24,25	13.3	[S_A + GL_C]
4	9	3	25	13.8	[S_A + GL_C]
4	10	3	25	13.6	[S_A + GL_C]
4	12	3	25	13.2	[S_A + GL_C]
4	3	0	19	13.1	[CYL_A]
4	3	1	19	12.9	[CYL_A]
4	3	2	19	12.1	[PL_A]
4	3	3	21	12.8	[PL_A]
4	3	4	22	13.1	[CYL_A]
4	3	5	22	12.9	[CYL_A]
4	3	6	23	13.1	[CYL_A]
4	3	8	24	13.1	[CYL_A]
4	3	10	25	13.2	[S_A]
4	3	12	27	13.8	[S_A]
4	3	14	27	13.5	[S_A]

matching self-consistent field theoretical (SCFT) values (valid for infinite chains) has not been done yet for multicomponent mikto-arm copolymers so any comparison can be only qualitative. However, we can say that in the compositional region where the two levels of coarse graining overlap, the CG1 high N molecules from Table 1 corresponds to χN values in the strong segregation regime while the CG2 lower N molecules from Table 2 corresponds to χN values in the intermediate to strong segregation regime. For the two reference structures in CG1 and CG2 respectively the χN values are 94.3 and 53.4 respectively.

3 Results

The reference structure from Fig. 2 self-assembles to a 3-colored perforated lamellar morphology illustrated in Fig. 3 (this structure is also published elsewhere[7] together with experimental evidence of the pattern). In this structure the red A phase makes lamellae with hexagonally arranged perforations. The layer to layer packing of the perforations is close-packed fcc. Through the center of the perforations protrusions of green C connect green adjacent layers. The blue B phase forms a lining between

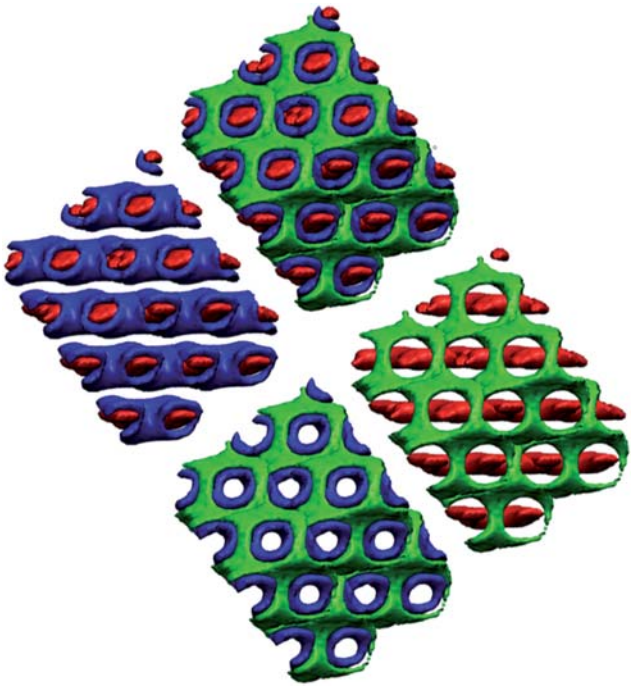

Fig. 3 3-colored perforated lamellar morphology [PL_A] obtained from DPD simulations of the reference structure A_7-(B_6-C_5)$_2$ and here split into pairs of components for visualization. All images are based on 8 ($2 \times 2 \times 2$) simulation boxes. The red A component forms a perforated lamellar phase with protrusions of green C and blue B. The blue B component forms a lining between the red A domains and the continuous green C phase. For more details see movie included as ESI.†

the red and green domains constrained by the topology of the molecular architecture. The details of the structure is best illustrated by the movie available as supplementary information. In Fig. 4 a summary of the results presented below are shown and it is clear that for comparable volume fractions of the A, B and C species the phase diagram is dominated by the morphology obtained for the reference structure which we will henceforth refer to as [PL_A]. In the following we will describe the details of the results from Fig. 4.

3.1 Varying the red A-component

Starting from when the red arm is completely removed (with arm length $n_A = 0$), the molecule corresponds roughly to a linear ABA triblock copolymer (CBC in our notation) and we find a lamellar morphology (denoted [LAM]) as expected for the investigated volume fractions,[36,37] an example of which is shown in Fig. 5(a). The lamellar phase is also found for $n_A = 1$, however, in some cases we also find a network phase where the red and blue domain form a single 3-connected gyroid-like core-shell network in a matrix of green. We denote this structure [GL_{AB}] and will discuss it in more detail below. When $n_A = 2$ we enter the domain of the [PL_A] phase persisting all the way to $n_A = 11$. At $n_A = 12$ a new lamellar phase [LAM_2] appears shown in Fig. 5(b). From the extended CG2 investigation results in Fig. 4 and Table 2 we find that increasing n_A further this lamellar phase is stable for the A chain significantly longer than the BC chains. We note

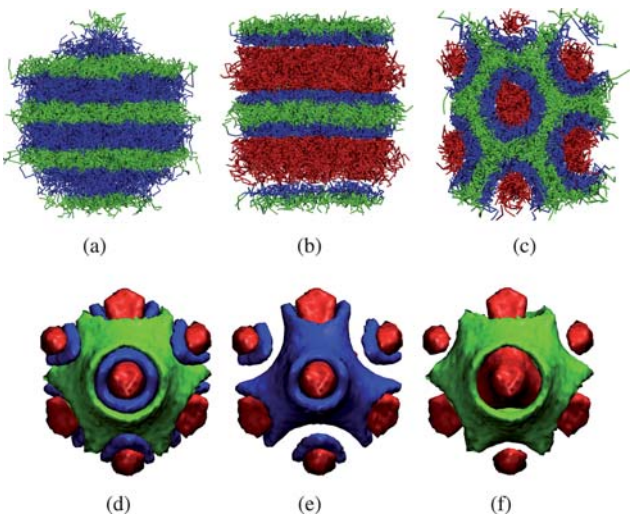

Fig. 5 Morphologies found when varying the length of the red A-arm. (a) [LAM] from A_0-(B_6-C_5)$_2$ star. (b) [LAM_2] from A_{12}-(B_3-C_3)$_2$ star. (c) [CYL_A] from A_3-(B_3-C_3)$_2$ star. (d–f) A node of the core-shell double diamond phase from A_9-(B_6-C_5)$_2$ star split into pairs of components for visualization. All snapshots are of a single simulation box.

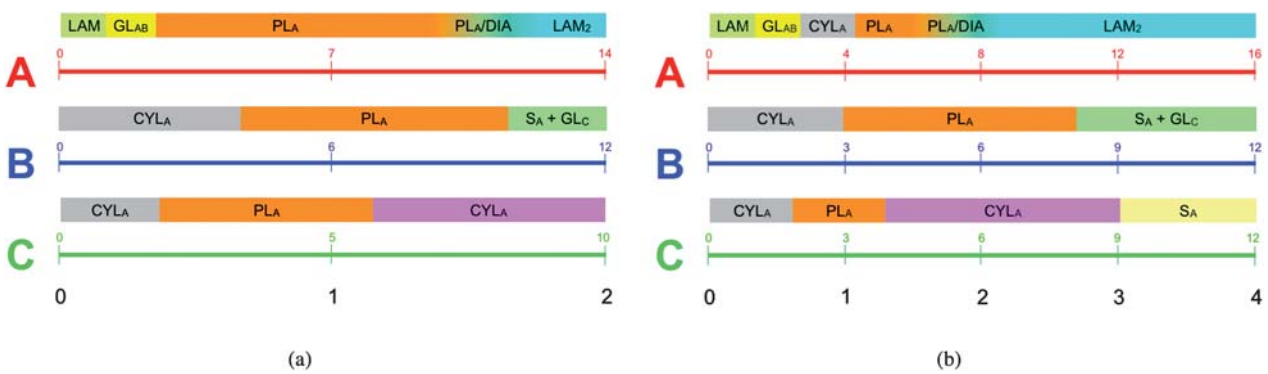

Fig. 4 Summary of the various phases found as a function of the relative volume fractions. Each colored axis represents the variation of the A (red), B (blue) or C (green) arm respectively relative to the reference structures of the CG1 and CG2 levels of coarse-graining. Colored numbers indicate the actual number of beads, the black numbers refer to the length relative to the relevant reference structure. (a) CG1 with reference A_7-(B_6-C_5)$_2$. (b) CG2 with reference A_4-(B_3-C_3)$_2$. See text for details of the different morphologies.

that close to the transition from the [PL_A] phase to [LAM_2] (for $n_A = 9,10,11$) we several times find a triple periodic cubic double diamond phase (denoted [DIA]) illustrated in Fig. 5(d–f). Here the red component forms the diamond networks, wrapped by the blue component and with the green component forming a triple periodic minimal surface between the two networks. As noted above in relation to the discussion of finite size effects, we cannot rule out that the double diamond phase is a box effect, however, phases with three-dimensional periodicity constitutes a notorious difficult issue in molecular simulation with periodic boundary conditions.[29] This is because that while these structures surely can be artificially stabilized by the cubic box, they will on the other hand never appear unless the box is commensurable with the periodicity of the phase itself, *i.e.* it has to 'fit' the box. Concerns like these are less relevant for morphologies of lower dimensional periodicity since these can reorient in the box to match the periodic boundary conditions. Given that we find this structure repeatedly we hypothesize that it could appear in the real copolymer system in the transition from the [PL_A] phase to [LAM_2]. If this can be verified experimentally it is quite surprising since normally a perforated lamellar phase will appear between bicontinuous and lamellar, not like here the bicontinuous between perforated lamellar and lamellar.[38]

Comparing the results of the two levels of coarse-graining, CG1 and CG2, we find overall agreement, except at low n_A where we find a cylindrical phase [CYL_A] in CG2 between [LAM]/[GL_{AB}] and [PL_A] (see Fig. 5(c)). The appearance of the [CYL_A] phase is not unexpected and the fact that we do not find it in the CG1 simulations indicate that there is an order-order transition between the two χN values represented by the two scenarios. The network phase [GL_{AB}] mentioned above is also found in CG2. In both scenarios it persists for different box sizes with the different structures being almost the same but not quite. This probably again reflects the issue of box commensurability discussed above. In all cases the red A minority component together with the junctions make a single 3-connected gyroid-like network, wrapped by the blue B component in a matrix of green C, see Fig. 6(a–c). In some cases the network appears to be a single gyroid network (a single 'srs' net following the naming convention from[39]) while in others it is unclear if it is some other 3-connected net. We note that a single 'srs' net has handedness so this structure could be a chiral morphology built from an achiral molecule. The formation of single network variants of the usual bicontinuous structures is a topic of recent interest,[40] so far with limited experimental verification. The clarification of whether this is an actual equilibrium structure and the exact nature of its net description as well as its formation in a real system are topics of ongoing work. Nevertheless, the fact that this structure appears for as short a chain as $n_A = 1$ indicates the tremendous importance of the star topology. The significance of the branching point has also recently been demonstrated experimentally in 3-armed polyethylene stars with the junction labeled allowing to follow the junction dynamics using neutron spin echo experiments. Here it is demonstrated that even a side chain one segment long severely alters junction point dynamics and rheological properties compared to a corresponding linear chain.[41]

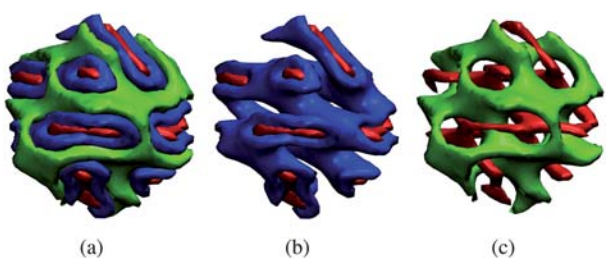

Fig. 6 Isosurface rendering of the network phase [GL_{AB}] from A_1-(B_3-C_3)$_2$ star. The red color represents the fused domain of the red minority component and the junction component. All snapshots are of (the same) single simulation box.

3.2 Varying the blue B-component

Starting again in the limit of $n_B = 0$ the molecule effectively becomes an AC_2 miktoarm copolymer and the resulting morphology is a cylindrical phase [CYL_A] in agreement with SCFT and previous DPD simulations.[3,30,42] This morphology persist until approximately $n_B = 4$ with the blue component wrapped around the red A cylinders and progressively thickening as n_B is increased. We state approximately since we can stabilize both [CYL_A] and [PL_A] at $n_B = 4$ indicating that this is right at the order-order transition between the two phases. An example of the [CYL_A] phase is shown in Fig. 7(a).

Upon increasing n_B we return to the [PL_A] morphology which persist until $n_B = 10$. When further increasing the size of the blue B-component we enter a region of a new phase which to our

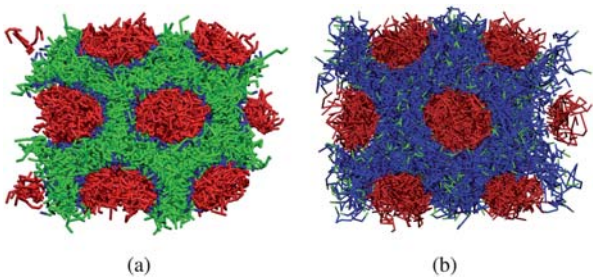

Fig. 7 Cylinder phases for n_B or $n_C = 1$. (a) From A_7-(B_1-C_5)$_2$ star. (b) From A_7-(B_6-C_1)$_2$ star.

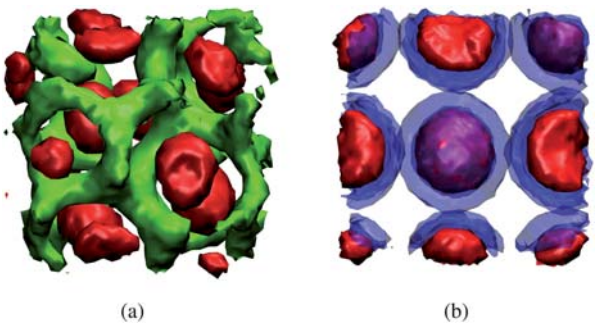

Fig. 8 (a) Novel morphology [S_A + GL_C] from A_4-(B_9-C_3)$_2$ star. Spheres of red A and a 3-connected gyroid-like network of green C components are embedded in a matrix of blue B component (not shown in image). (b) Close-packed sphere packing [S_A] from A_4-(B_3-C_{14})$_2$ star viewed edge-on. Red A spheres covered with blue B are embedded in a matrix of the green C component (not shown in image).

knowledge is also unreported in the literature. The red A-component now forms closed globular domains while the green C-component forms a continuous 3-connected gyroid-like network phase, both embedded in a matrix of the blue B-component, see Fig. 8(a). We denote this structure [S_A + GL_C]. As discussed above with the [GL_{AB}] this is potentially a chiral structure if the 3-connected network forms a 'srs'-net. The [S_A + GL_C] structure is also found in the CG2 simulations which are generally in agreement with the CG1 results.

3.3 Varying the green C-component

As when varying the B-component, the $n_C = 0$ adopts a cylindrical morphology. This also appears for $n_C = 1$ as shown Fig. 7(b). At $n_C = 2$ we enter the region of the [PL_A] phase which persists until $n_C = 5$ after which we return to structures with cylinders of A. Thus, the green C-component shows the most restricted region of stability for the [PL_A] morphology. For the rest of the CG1 simulations, *i.e.* $n_C = 6$ to 10, the cylindrical phases persist, but from the CG2 simulations we find that when increasing the volume fraction of the blue component further we reach structures with fcc sphere packings of A, [S_A], covered with a layer of B and embedded in a matrix of green C component, see Fig. 8(b). Overall, there is good agreement between the CG1 and CG2 scenarios when varying the length of the green C-component.

4 Conclusions

The self-assembly of a range of compositionally different $A(BC)_2$ mikto-arm star copolymers has been simulated using dissipative particle dynamics simulations. The simulations reveal that in the region where all polymer species are not to different in size the equilibrium morphology is a novel 3-colored perforated lamellar pattern recently identified experimentally[7] which is robust in terms of modest composition and interaction variations as revealed by varying relative arms lengths and simulating at both intermediate and strong segregation. From the latter we conclude that just as shown for both linear AB and AB_2 mikto-arm copolymers the composition dominates the microstructure formation in complex copolymer systems.[30] Further, we stress that the increased compositional stability of the perforated lamellar pattern compared to diblock copolymer systems is a result of the complex molecular architecture. In the limits where the size of one block becomes either small or large, the resulting morphologies usually follow those expected from AB_2 mikto-arm or ABA linear copolymers respectively. Two notable exceptions appear: one is when expanding the blue B-component where a novel morphology appears consisting of spheres of A and a 3-connected gyroid-like network of C embedded in a matrix of B and the other is for short red A-arms where a structure built from a single gyroid-like core-shell network of A, wrapped in B and embedded in a matrix of C. The clarification of whether these structures can be formed experimentally is the topic of ongoing work.

5 Acknowledgments

The author wish to thank Nikos Hadjichristidis for inspiration to explore the $A(BC)_2$ mikto-arm copolymer system and Kell Mortensen, Stephen Hyde and Liliana de Campo for useful comments to the manuscript.

References

1 N. Hadjichristidis, S. Pispas and G. Floudas, *Block copolymers: synthetic strategies, physical properties and applications*, Wiley, 2003.
2 I. Hamley, *The physics of block copolymers*, Oxford University Press, 1998.
3 M. W. Matsen and F. Bates, *Macromolecules*, 1996, **29**, 1091.
4 N. Hadjichristidis, H. Iatroua, M. Pitsikalisa, S. Pispas and A. Avgeropoulos, *Prog. Polym. Sci.*, 2005, **30**, 725–782.
5 Y. Mogi, K. Mori, Y. Matsushita and I. Noda, *Macromolecules*, 1992, **25**, 5412–5415.
6 P. Tang, F. Qiu, H. Zhang and Y. Yang, *Phys. Rev. E: Stat., Nonlinear, Soft Matter Phys.*, 2004, **69**, 8434–8438.
7 J. J. K. Kirkensgaard, P. Fragouli, N. Hadjichristidis and K. Mortensen, In Review.
8 K. Mortensen and M. E. Vigild, *Macromolecules*, 2009, **42**, 1685–1690.
9 K. Almdal, K. Koppi, F. Bates and K. Mortensen, *Macromolecules*, 1992, **25**, 1743–1751.
10 T. Hashimoto, S. Koizumi, H. Hasegawa, T. Izumitani and S. Hyde, *Macromolecules*, 1992, **25**, 1433–1439.
11 I. W. Hamley, K. A. Koppi, J. H. Rosedale, F. S. Bates, K. Almdal and K. Mortensen, *Macromolecules*, 1993, **26**, 5959–5970.
12 R. J. Spontak, S. D. Smith and A. Ashraf, *Macromolecules*, 1993, **26**, 956–962.
13 M. Disko, K. S. Liang, S. K. Behal, R. J. Roe and K. J. Jeon, *Macromolecules*, 1993, **26**, 2983–2986.
14 I. W. Hamley, M. D. Gehlsen, A. K. Khandpur, K. A. Koppi, J. H. Rosedale, M. F. Schulz, F. S. Bates, K. Almdal and K. Mortensen, *J. Phys. II*, 1994, **4**, 2161–2186.
15 M. W. Matsen and M. Schick, *Phys. Rev. Lett.*, 1994, **72**, 2660–2663.
16 S. Qi and Z. G. Wang, *Phys. Rev. Lett.*, 1996, **76**, 1679–1782.
17 S. Qi and Z. G. Wang, *Phys. Rev. E: Stat. Phys., Plasmas, Fluids, Relat. Interdiscip. Top.*, 1997, **55**, 1682–1697.
18 M. W. Matsen and F. S. Bates, *J. Chem. Phys.*, 1997, **106**, 2436–2448.
19 M. E. Vigild, K. Almdal, K. Mortensen, I. W. Hamley, J. P. A. Fairclough and A. J. Ryan, *Macromolecules*, 1998, **31**, 5702–5716.
20 D. A. Hajduk, R. H. Ho, M. A. Hillmyer, F. S. Bates and K. Almdal, *J. Phys. Chem. B*, 1998, **102**, 1356–1363.
21 C. Y. Wang and T. P. Lodge, *Macromolecules*, 2002, **35**, 6997–7006.
22 L. Zhu, P. Huang, W. Y. Chen, X. Weng, S. Z. D. Cheng, Q. Ge, R. P. Quirk, T. Senador, M. T. Shaw, E. L. Thomas, B. Lotz, B. S. Hsiao, F. Yeh and L. Liu, *Macromolecules*, 2003, **36**, 3180–3188.
23 I. W. Hamley, V. Castelletto, O. O. Mykhaylyk and A. J. Gleeson, *J. Appl. Crystallogr.*, 2004, **37**, 341–344.
24 R. Eskimergen, K. Mortensen and M. E. Vigild, *Macromolecules*, 2005, **38**, 1286–1291.
25 V. H. Mareau, S. Akasaka, T. Osaka and H. Hasegawa, *Macromolecules*, 2007, **40**, 9032–9039.
26 P. Hoogerbrugge and J. M. V. Koelman, *Europhys. Lett.*, 1992, **19**, 155.
27 P. Espanol and P. Warren, *Europhys. Lett.*, 1995, **30**, 191.
28 R. Groot and P. Warren, *J. Chem. Phys.*, 1997, **107**, 4423.
29 R. Groot and T. Madden, *J. Chem. Phys.*, 1998, **108**, 8713.
30 C. Huang and H. Yu, *Polymer*, 2007, **48**, 4537–4546.
31 H. J. Limbach, A. Arnold, B. A. Mann and C. Holm, *Comput. Phys. Commun.*, 2006, **174**, 704–727.
32 J. J. K. Kirkensgaard and S. Hyde, *Phys. Chem. Chem. Phys.*, 2009, **11**, 2016–2022.
33 W. Humphrey, A. Dalke and K. Schulten, *J. Mol. Graphics*, 1996, **14**, 33–38.
34 C. Soto-Figueroa, M. Rodriguez-Hidalgo and J. Martinez-Magadan, *Chem. Phys. Lett.*, 2008, **460**, 507–511.
35 C. Huang, H. Fang and C. Lin, *Phys. Rev. E: Stat., Nonlinear, Soft Matter Phys.*, 2008, **77**, 031804.
36 M. W. Matsen and R. Thompson, *J. Chem. Phys.*, 1999, **111**, 7139.
37 B. Abu-Sharkh and A. AlSunaidi, *Macromol. Theory Simul.*, 2006, **15**, 507–515.
38 S. T. Hyde, in *Handbook of Applied Surface and Colloid Chemistry*, John Wiley and Sons, Ltd, 2001, ch. 16.

39 M. O'Keeffe, M. Peskov, S. Ramsden and O. Yaghi, *Acc. Chem. Res.*, 2008, **41**, 1782–1789.
40 M. Fuhrmans, V. Knecht and S. Marrink, *J. Am. Chem. Soc.*, 2009, **131**, 9166–9167.
41 M. Zamponi, W. Pyckhout-Hintzen, A. Wischnewski, M. Monkenbusch, L. Willnert, G. Kali and D. Richter, *Macromolecules*, 2010, **43**, 518–524.
42 H. Qian, L. Chen, Z. Lu, Z. Li and C. Sun, *J. Chem. Phys.*, 2006, **124**, 014903.